*J. Fluid Mech.* (1980), *vol.* 100, *part* 1, *pp.* 129–146
*Printed in Great Britain*



# Two-layer model for shallow horizontal convective circulation

By DOMINIQUE N. BROCARD† AND DONALD R. F. HARLEMAN

R. M. Parsons Laboratory for Water Resources and Hydrodynamics, Massachusetts Institute of Technology, Cambridge, Massachusetts 02139

(Received 10 July 1978)

This paper discusses experiments and a theoretical model for the convective circulation driven by a surface buoyancy flux in a horizontal layer of fluid. The layer is closed at one end and, at the other end, the buoyancy has a fixed value over a given depth. Such circulation occurs in side arms of cooling lakes used for waste-heat disposal from power generation. Some geophysical circulations, such as in the Red Sea, are also of the above type.

The experiments were done in a 35 ft long flume using heat transfer between the heated water and the atmosphere to generate the surface buoyancy flux. The observed circulation was characterized by two distinct layers flowing in opposite directions and separated by a density interface. For upper-layer depths less than about half the total depth at the open end, the downflow was observed to be concentrated near the closed end. Circulation flowrates and vertical temperature profiles were measured.

The theoretical model uses a 'two-layer' approach. The mass, momentum, and buoyancy conservation equations are integrated vertically on each side of the interface. Mass and buoyancy transfer across the interface are neglected. The interfacial shear stress is proportional to the square of the difference of the average layer velocities. For small layer densimetric Froude numbers, the free surface is shown to be approximately horizontal and the problem reduces to one ordinary differential equation for the thickness of the upper layer. General solutions of this interface equation are presented for horizontal and sloping bottoms. Different configurations are possible depending on the nature of the singular points which occur in the phase plan.

For the convective circulation, the interface is shown to go through a singular point. This condition leads to a simple analytical solution for the circulation flowrate in the case of constant surface buoyancy flux and horizontal bottom. This solution compares well with the experimental data and with measurements on the Red Sea circulation.

## 1. Introduction

The type of convective circulation considered in this paper is shown schematically in figure 1. It is driven by a surface buoyancy flux, $B$, in a horizontal layer of fluid closed at one end and at the other end of which the buoyancy, $b = -g(\rho - \rho_R)/\rho_R$,

† Present address: Alden Research Laboratory, Worcester Polytechnic Institute, Holden, Massachusetts, 01520.

0022–1120/80/4515–1760 $02.00 

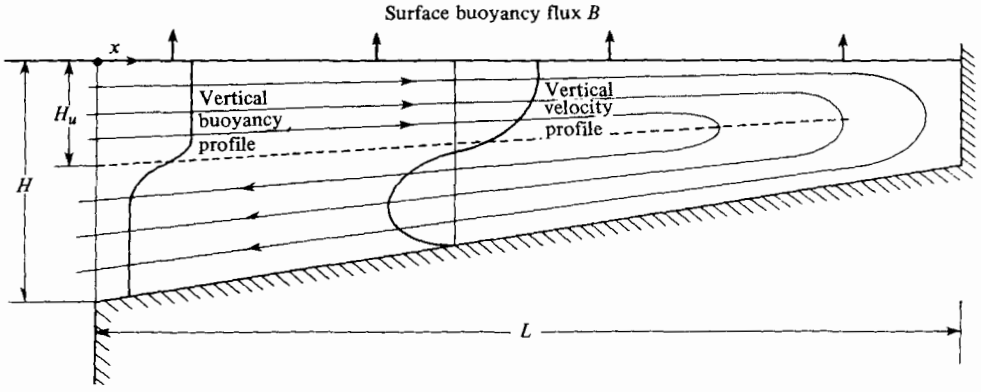


FIGURE 1. Shallow horizontal convective circulation.

has a fixed value $b_0$ over a depth $H_u$ from the top. In the definition of $b$, $g$ is the acceleration of gravity, $\rho$ is the local fluid density (averaged over turbulent fluctuations), and $\rho_R$ is a reference density. The length of the layer is $L$, the depth at the open end is $H$, and the possibility of a constant bottom slope, $S$, is included. Only the case of a shallow layer of fluid is considered in which the upper current is vertically well-mixed by the turbulence resulting from the unstability generating surface buoyancy flux. Lateral uniformity is assumed, leading to a two-dimensional problem in the vertical plane.

The circulation described above occurs in the side arms of cooling lakes used for the disposal of waste heat from power generation. Side arms occur from the flooding of tributary valleys when the cooling lake was formed by daming a river. Knowledge of the circulation characteristics is required for the prediction of the thermal response of the lake to the waste heat loading. In this case, the surface buoyancy flux, $B$, is due to the surface heat flux, $\Phi$ (energy per unit area per unit time) and is given by

$$B = g\beta\Phi/\rho C_p \tag{1}$$

in which $\beta = (-1/\rho)\,\partial\rho/\partial T$ is the thermal expansion coefficient of the fluid there, water), and $C_p$ is its specific heat. The net heat flux across a water surface is the algebraic sum of individual fluxes due to radiation, both from the surroundings and from the water surface, convection, and evaporation. The net flux is, therefore, dependent upon the water surface temperature, $T_s$, and various parameters characterizing the conditions above the surface. For outdoor situations, the latter are typically the air temperature, the relative humidity, the solar flux, and angle above the water surface (which affects reflexion), the cloud cover (which affects atmospheric radiation), and the wind speed. Each of the individual heat fluxes can be calculated, with varying degrees of empiricism, see Ryan, Harleman & Stolzenbach (1974), but the following expression, introduced by Edinger & Geyer (1965) provides a useful approximate dependence of the net flux upon the water surface temperature, given a set of meterological conditions:

$$\Phi = \rho C_p k(T_s - T_E). \tag{2}$$

In this expression, $\Phi$ is counted positively upwards, $k$ is a heat-flux coefficient, and $T_E$ is the equilibrium temperature. Equations (1) and (2) lead to

$$B = k(b_s - b_E) \tag{3}$$

where $b_s$ and $b_E$ are the values of buoyancy corresponding to $T_s$ and $T_E$. By taking the reference density, $\rho_R$, used in the definition of buoyancy equal to the density of water, $\rho_E$, at equilibrium temperature, (3) further simplifies to

$$B = kb_s. \tag{4}$$

Both this case and that of a constant surface buoyancy flux will be considered in the analysis presented in § 3.

Another example of the type of convective circulation under study here is that of the Red Sea. In this case, the surface buoyancy flux is the result of the surface heat flux and the increase in salt concentration resulting from evaporation. Phillips (1966) presented a similarity analysis of this circulation assuming a constant surface buoyancy flux. The analysis leads to the two-dimensional distributions of the velocity and buoyancy which, however, involve unknown similarity functions. The measured vertical buoyancy profiles presented by Phillips show rather smooth variations and in particular do not exhibit the sharp gradient observed in cooling lake side arms and which is an essential element of the two-layer model developed here. The results of the two analyses do, however, present interesting similarities which will be returned to. Another major difference is the fact that Phillips does not impose any boundary condition at the entrance of the circulation region, at $x = 0$ in figure 1. The experiments described in the following section and the later analysis show that the depth, $H_u$, of the thermocline at $x = 0$ is a major controlling parameter.

## 2. Experimental study

A drawing of the set-up used for the circulation experiments is presented in figure 2. The set-up was composed of an insulated flume 2·5 ft wide, 1 ft deep, and of adjustable length up to 35 ft, connected to a large rectangular basin designed to provide fixed entrance boundary conditions, in addition to the abrupt expansion–contraction present in the field situations described in § 1. The driving surface buoyancy flux was produced by the heat flux associated with the atmospheric cooling of heated water. This heated water was introduced at the surface of the large basin through a discharge device designed to minimize the horizontal momentum and mixing. This device consisted of a horizontal board, topped with rubberized horsehair as energy dissipator. An equal amount of water was withdrawn through an outflow manifold placed transversally in the basin $\frac{1}{2}$ inch above the floor. The outflow rate was controlled by a cylindrical outflow weir which ensured a constant water level in the system and, therefore, equal inflow and outflow.

Starting from a uniform temperature in the system, a flow of prescribed magnitude and temperature was introduced. This procedure differs from the initial formulation of the problem in which the thermocline depth is fixed and the circulation flowrate is unknown. However, at steady state, the thermocline depth, $H_u$, established itself in the basin, and was then measured. The time required to reach steady state was

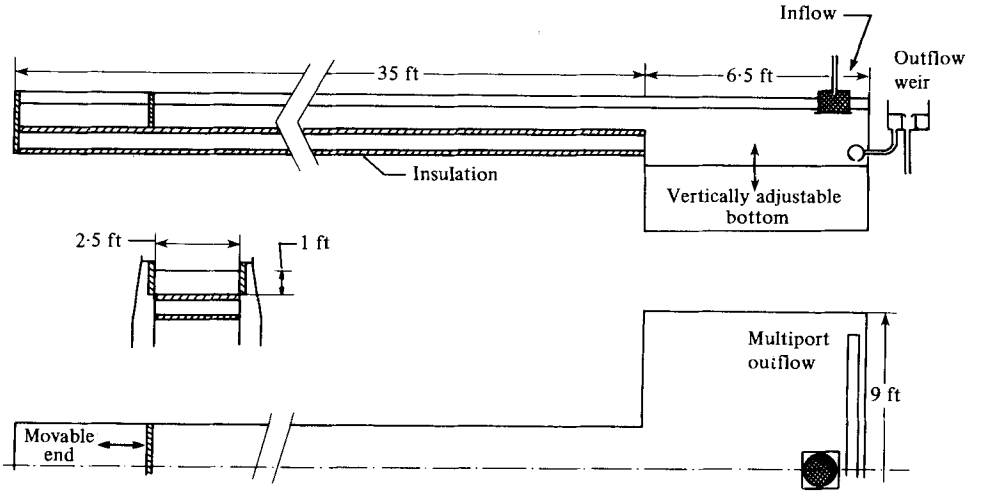


FIGURE 2. Schematic drawing of experimental set-up.

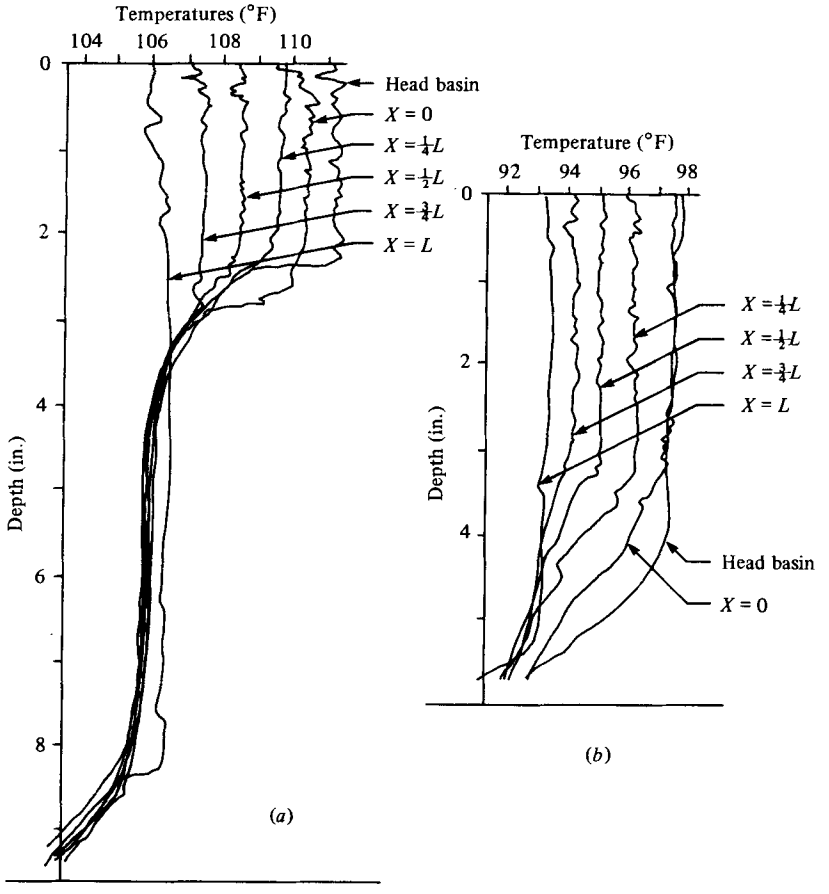


FIGURE 3. Vertical temperature profiles for two experimental runs. (*a*) $L = 34{\cdot}6$ ft, $T_E = 71$ °F, $k = 2{\cdot}8 \times 10^{-5}$ ft s$^{-1}$. (*b*) $L = 34{\cdot}6$ ft, $T_E = 70$ °F, $k = 2{\cdot}1 \times 10^{-5}$ ft s$^{-1}$.

typically 6 to 8 hours. The flow field and the temperature distribution in the side arm were then measured.

Temperatures were measured in two ways: A set of 50 stationary thermistor probes distributed in vertical arrays on the flume centre-line recorded instantaneous temperature distributions in the system at fixed points. Also, continuous vertical temperature profiles were obtained via a motorized fast response thermistor probe linked to an $x, y$ plotter. Vertical temperature profiles obtained in this way are reproduced in figure 3 for two experimental runs. The velocity field was explored by taking successive photographs, through the Plexiglas side walls of the flume, of the traces produced by the dissolution of dye crystals dropped in the water.

The laboratory meteorological parameters needed to determine the heat flux across the water surface are the air temperature and relative humidity. Both were monitored during the experimental runs. The surface heat flux was then calculated using the concepts and formulae recommended by Ryan *et al.* (1974). To check these calculations, the equilibrium temperature was also measured in a shallow bucket, insulated on the sides and bottom and left permanently in the vicinity of the flume. Comparison with computed values was satisfactory. Full details on these calculations, which lead to the values of $k$ and $T_E$, are presented by Brocard, Jirka & Harleman (1977).

The majority of the experiments were performed for the basic case of a side arm with a horizontal bottom. The effects of a bottom slope on the circulation were studied in an additional series of runs with a longitudinally constant bottom slope reaching the surface at the closed end so that $S = H/L$. The parameters and results of the runs are presented in tabular form by Brocard *et al.* (1977). They are plotted in dimensionless form in figure 11, where they are compared with the predictions of the mathematical model developed thereafter.

The major qualitative results and observations derived from these experiments are as follows:

1. With the low velocities encountered in the experiments, the Reynolds number of the flow remained small and shear generated turbulence was absent so that only the upper layer was turbulent, because of the surface cooling instability. This fact appears in the vertical temperature profiles obtained with the travelling probe which are presented in figure 3. They generally exhibit a vertically well-mixed upper layer and a very smooth profile in the lower layer, typical of laminar conditions.

2. Figure 3 shows the two possible circulation regimes set forth by the experiments. For shallow entrance upper layer depths (approximately $H_u/H$ less than 0·5), the temperature profiles in the lower layer fall almost on top of each other, indicating a longitudinally constant temperature and consequently very little downflow before the closed end. By contrast, runs with deep upper layer, show varying lower layer temperatures, which can only be attributed to continuous downflow from the upper layer. These results are confirmed by the flow measurements. For shallow upper layer, the layer flow is actually observed to slightly increase towards the end (approximately 10 % from the entrance to half length) pointing to some turbulent entrainment by the upper layer. For deeper entrance upper-layer depths, flow measurements indicate a decrease of the flow of up to 30 % between the entrance and half-length point.

3. When the upper-layer depth was shallow at the entrance, it increased slightly towards the end of the side arm whereas, when it was deep at the entrance, the upper layer decreased rapidly to final values close to half depth.

4. The interfacial and bottom heat flux were calculated and found to be much smaller than the surface heat flux.

Overall, the experimental results and observations point to the 'two-layer' structure of the circulation with a large temperature and, therefore, buoyancy gradient separating two layers and little flow across this interface. This is particularly true for the case of shallow upper layer where the downflow is restricted to the close neighbourhood of the closed end. The case of deep upper layer presents significant downflow starting at the entrance, and if this does not preclude the application of two-layer flow theory, it poses the additional problem of determining the magnitude and distribution of the downflow.

## 3. Two-layer model for stratified flows

Based upon the experimental observations, a model involving the 'two layer' scheme is developed for the buoyancy-flux driven circulation. First, however, the governing equations are derived and studied in general terms. The two-layer approach is based on the fact that a sharp stable buoyancy gradient tends to inhibit vertical transfers of momentum and mass and can, therefore, be seen as an interface between two layers. This schematization, which is shown in figure 4, was introduced by Schijf & Schonfeld (1953) and was successfully applied to a number of stratified flow problems in hydraulics (Rigter 1970; Hsu & Stolzenbach 1975), and in oceanography (Welander 1974; Long 1975). The equations governing two-layer flows are obtained by vertically integrating the mass, momentum and buoyancy conservation equations on each side of the interface and expressing them in terms of layer-averaged variables. This procedure leads to the following:

$$\frac{dq_1}{dx} = -\frac{dq_2}{dx} = W_i, \tag{5}$$

$$-\alpha_1 \frac{q_1^2}{h_1^3}\frac{dh_1}{dx} + \left[\alpha_1 \frac{2q_1}{h_1^2} - \frac{U_i}{h_1^2}\right] W_i = \frac{h_1}{2}\frac{db_1}{dx} + (b_1 - g)\frac{d(h_1+h_2+h_b)}{dx} - \frac{\tau_i}{\rho_R h_1}, \tag{6}$$

$$-\alpha_2 \frac{q_2^2}{h_2^3}\frac{dh_2}{dx} - \left[\alpha_2 \frac{2q_2}{h_2^2} - \frac{U_i}{h_2}\right] W_i = h_1 \frac{db_1}{dx} + \frac{h_2}{2}\frac{db_2}{dx} + (b_2 - g)\frac{d(h_1+h_2+h_b)}{dx} - (b_1 - b_2)\frac{dh_1}{dx} + \frac{\tau_i - \tau_0}{\rho_R h_2}, \tag{7}$$

$$q_1 \frac{db_1}{dx} - W_i(b_1 - b_i) = -B + B_i, \tag{8}$$

$$q_2 \frac{db_2}{dx} + W_i(b_2 - b_i) = B_i, \tag{9}$$

with

$$b_i = b_1 \quad \text{for} \quad W_i < 0, \quad b_i = b_2 \quad \text{for} \quad W_i > 0.$$

Here $h_1$ and $h_2$ are the upper- and lower-layer depths and $h_b$ is the bottom elevation above a horizontal datum, $q_1$ and $q_2$ are the upper- and lower-layer flowrates per unit width defined by

$$q_1 = \int_{h_b}^{h_b+h_2} u\,dz \quad \text{and} \quad q_2 = \int_{h_2+h_b}^{h_1+h_2+h_b} u\,dz,$$

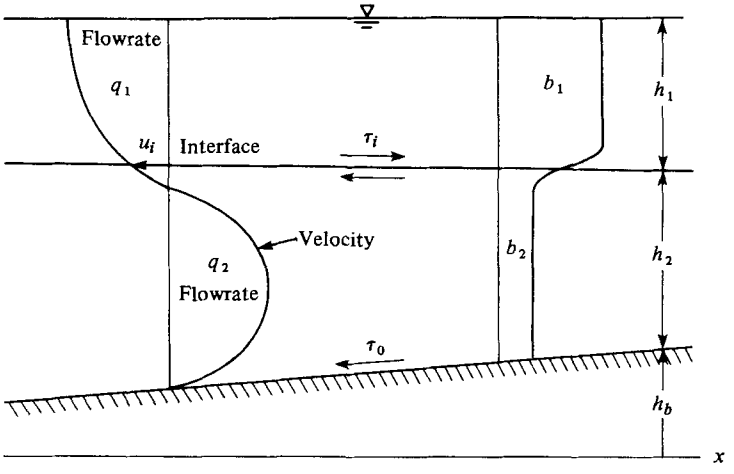


FIGURE 4. Schematized two-layer flow.

and $b_1$ and $b_2$ are the vertically averaged layer buoyancies. All these quantities are functions of the longitudinal abscissa $x$. The momentum-flux coefficients $\alpha_1$ and $\alpha_2$ are assumed to be constant and are defined by

$$\alpha_1 = \frac{h_1 \int_{h_2+h_b}^{h_1+h_2+h_b} u^2\,dz}{\left[\int_{h_2+h_b}^{h_1+h_2+h_b} u\,dz\right]^2}; \quad \alpha_2 = \frac{h_2 \int_{h_b}^{h_b+h_2} u^2\,dz}{\left[\int_{h_2+h_b}^{h_1+h_2+h_b} u\,dz\right]^2}.$$

For turbulent flows, these coefficients are typically of the order of 1·05 and can be approximated by unity. For laminar velocity profiles, as present in the experiments described in § 2, $\alpha_1$ and $\alpha_2$ can reach significantly higher values and are kept here for generality. The bottom shear stress $\tau_0$ is traditionally expressed in terms of the lower-layer flow rate as follows

$$\tau_0 = \tfrac{1}{8} f_0 \rho (q_2/h_2)^2, \tag{10}$$

where $f_0$ is a friction factor which depends on the Reynolds number, $R = q_2/\nu$, and the bottom roughness. For laminar flow, $f_0 = 48/R$, while for turbulent flow, $f_0$ depends on the bottom roughness only and a typical value is 0·02.

A number of interface related quantities have been introduced which need to be expressed in terms of the layer-averaged variables. The special nature of the interface is expected to make this possible through approximate relationships. The interfacial quantities to be estimated are the interfacial buoyancy flux, $B_i$, the horizontal and vertical components of the velocity at the interface, $U_i$ and $W_i$, and the interfacial shear stress, $\tau_i$.

The interfacial buoyancy flux, $B_i$, is due to molecular diffusion and, when one or both layers are turbulent, to the resulting entrainment of fluid from the other layer. Estimation of the former requires the knowledge of the thickness $h^*$ of the buoyancy gradient while the latter can be calculated based upon the experimental studies of Lofquist (1960) and Moore & Long (1971). These will also lead to the value of $W_i$, which represents the net entrained mass flux across the interface. Both molecular and

turbulent buoyancy and mass transfer across the interface play only a secondary role in the type of flows considered herein and will, therefore, be left out for simplicity. This approximation also avoids the need for estimating $U_i$. The interfacial shear stress, $\tau_i$, is typically expressed as follows, by analogy with equation (10):

$$\tau_i = \tfrac{1}{8} f_i \rho (q_1/h_1 - q_2/h_2). \tag{11}$$

The somewhat limited basis for this expression leads to difficulties in the estimation of the interfacial friction factor, $f_i$. For turbulent flows, $f_i$ would be expected to depend on the stability characteristics of the interface, measured by a Richardson number or rather, in the two-layer context, by the densimetric Froude numbers of the layers:

$$F_1 = \frac{\alpha_1 q_1}{((b_1 - b_2) h_1^3)^{\frac{1}{2}}}, \quad F_2 = \frac{\alpha_2 q_2}{((b_1 - b_2) h_2^3)^{\frac{1}{2}}}.$$

Such a dependence has, however, not yet been clearly established. Karelse (1974) reviewed experimental evaluations and correlation of the interfacial friction factor and recommends values of $f_i = 0{\cdot}006$ to $0{\cdot}012$ for counterflows.

Utilizing these approximate expressions, including $W_i \simeq 0$, and for the case of small buoyancy difference between the layers ($b_1 - b_2 = \Delta b \ll g$), the two-layer momentum equations, equations (6) and (7), can be transformed to the following, in which terms of the order $\Delta b/g$ are neglected:

$$\frac{dh_1}{dx} = \frac{\dfrac{dh_b}{dx} F_2^2}{1 - F_1^2 - F_2^2} + \frac{\dfrac{db_1}{dx}\dfrac{h_1}{2} + \dfrac{db_2}{dx}\dfrac{h_2}{2} + \dfrac{f_i}{8}\left(\dfrac{q_1}{h_1} - \dfrac{q_2}{h_2}\right)^2 \left(\dfrac{1}{h_1} + \dfrac{1}{h_2}\right) - \dfrac{f_0}{8}\dfrac{q_2^2}{h_2^3}}{\Delta b\,[1 - F_1^2 - F_2^2)}, \tag{12}$$

$$\frac{d(h_1 + h_2)}{dx} = -\frac{dh_b}{dx}. \tag{13}$$

Also implied in the approximations leading to the above equations is the fact that the layer densimetric Froude numbers, $F_1$ and $F_2$, remain of order one at most. This assumption is verified for the types of stratified flows with stable interface under consideration here. As shown by equation (13), these flows will be characterized by a practically horizontal, free surface.

Characteristic values for the total depth, $H$, the flow rate per unit width, $q_0$ and the horizontal distance, $L$, are now introduced and used to define new dimensionless variables:

$$X = \frac{x}{L}, \quad h = \frac{h_1}{H}, \quad \mathscr{H} = \frac{h_1 + h_2}{H}, \quad s = \frac{dh_b}{dx}\frac{L}{H},$$

$$q = \frac{q_1}{q_0}, \quad \Delta q = \frac{q_1 - q_2}{q_0}, \quad r_1 = \frac{b_1}{b_0}, \quad r_2 = \frac{b_2}{b_0}.$$

If, as already assumed, the interfacial flow is neglected ($W_i = 0$), the continuity equations, (5), states that the layer flowrates $q_1$ and $q_2$ are constant and if $q_0$ is taken equal to the upper layer flow, it follows that $q = 1$. The flow differences, $\Delta q$, is also a

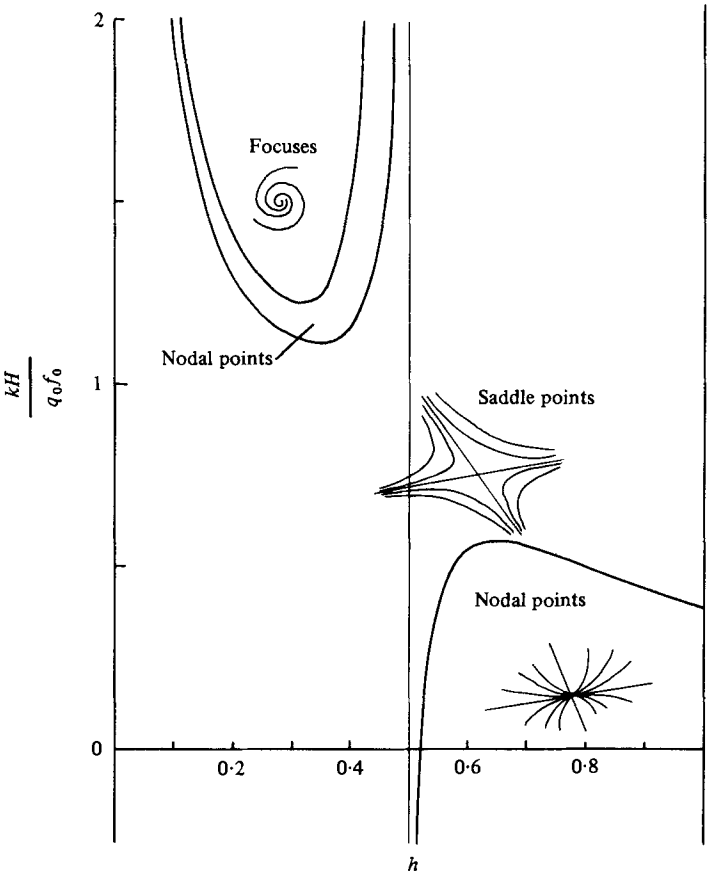


FIGURE 5. Nature of singular points of the interface equation for the case of a horizontal bottom.

constant which becomes equal to zero in the case of equal counterflow. In dimensionless form, the momentum equation becomes:

$$\frac{dh}{dX} = \frac{sF_E^2\dfrac{\alpha_2(\Delta q-1)^2}{(\mathscr{H}-h)^3} - \dfrac{dr_1}{dX}\dfrac{h}{2} - \dfrac{dr_2}{dX}\dfrac{\mathscr{H}-h}{2}}{(r_1-r_2) - F_E^2\left[\dfrac{\alpha_1}{h^3}+\dfrac{\alpha_2(\Delta q-1)^2}{(\mathscr{H}-h)^3}\right]}$$

$$\frac{-F_E^2\dfrac{f_0 L}{8H}\left[\epsilon_i\alpha\left(\dfrac{1}{h}-\dfrac{\Delta q-1}{\mathscr{H}-h}\right)^2\left(\dfrac{1}{h}+\dfrac{1}{\mathscr{H}-h}\right)-\epsilon_0\dfrac{(\Delta q-1)^2}{(\mathscr{H}-h)^3}\right]}{(r_1-r_2) - F_E^2\left[\dfrac{\alpha_1}{h^3}+\dfrac{\alpha_2(\Delta q-1)^2}{(\mathscr{H}-h)^3}\right]}, \quad (14)$$

$$\frac{d\mathscr{H}}{dX} = -s, \quad (15)$$

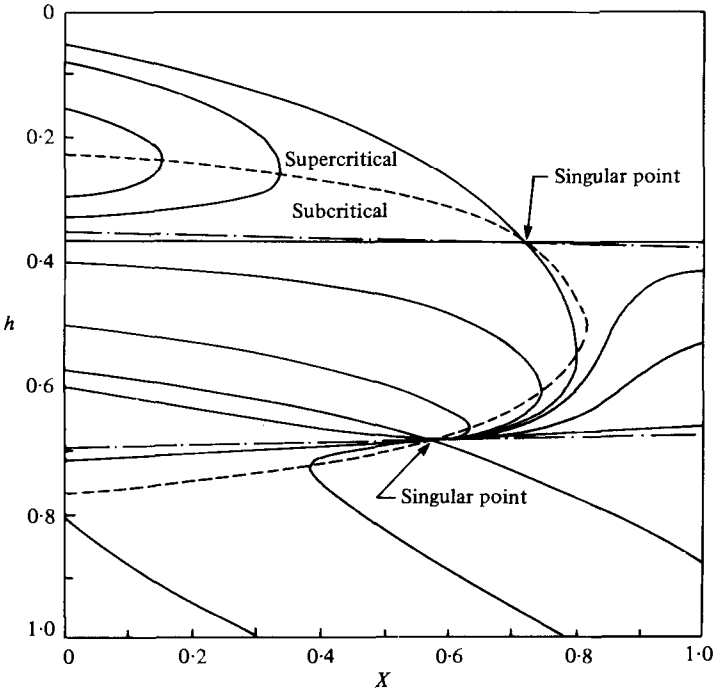


FIGURE 6. Solutions of the interface equation with horizontal bottom and $F_E^2 = 1{\cdot}28 \times 10^3$, $q_0/kL = 8, f_0 L/H = 3$. – – –, Locus of critical point; —· —, locus of points with zero interface slope.

in which $\alpha = f_i/f_0$, $\epsilon_0 = \text{sgn}\ (\Delta q - 1)$, $\epsilon_i = \text{sgn}\ (2 - \Delta q)$ and $F_E^2 = q_0^2/b_0 H^3$. The buoyancy conservation equation for the upper layer, (8), becomes:

$$\frac{dr_1}{dX} = -\frac{BL}{q_0 b_0}. \tag{16}$$

If equation (4) is used with $b_s = b_1$ for the surface buoyancy flux $B$, and $b_0$ is the upper-layer buoyancy at $X = 0$, the previous equation gives:

$$r_1 = \exp -\frac{kL}{q_0} X. \tag{17}$$

For the case of constant surface buoyancy flux, $B = kb_0$ leads to

$$r_1 = \left(1 - \frac{kL}{q_0} X\right), \tag{18}$$

which is the first term in the linear expansion of (17) for small $kL/q_0$. The buoyancy, $r_2$, of the lower layer remains constant.

In the foregoing equations for two-layer flows with surface buoyancy flux, it is equation (14) which governs the dynamics of the system. This equation is of the type $dh/dX = P(X,h)/Q(X,h)$, where $P$ and $Q$ are functions of both $X$ and $h$. Points $(X_c, h_c)$ such that $Q(X_c, h_c) = 0$ correspond to infinite interface slope and are, in the context of two-layer flows, called critical points. Although it is not clearly apparent

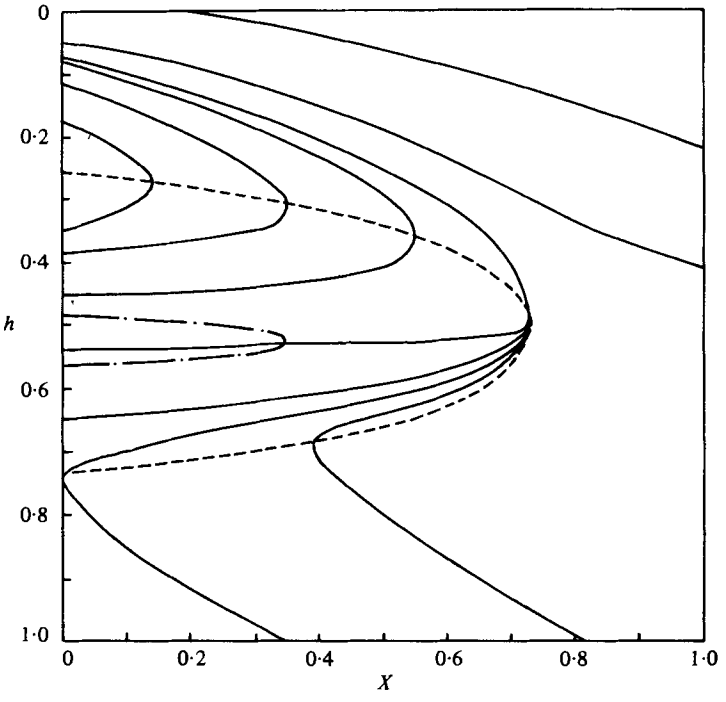


FIGURE 7. Solutions of the interface equation with horizontal bottom and $F_E^2 = 1{\cdot}28 \times 10^3$, $q_0/kL = 12{\cdot}8$, $f_0 L/H = 3$. – – –, Locus of critical points; —·—, locus of points with zero interface slope.

from the form of $Q(X, h)$ in equation (15), the critical condition, ($Q = 0$) is equivalent to:

$$F_1^2 + F_2^2 = 1. \tag{19}$$

Critical points play an important role in two-layer flows. With an infinite interface slope, critical points will only occur at remarkable sections in the flow such as abrupt expansion and contractions, where equation (21) furnishes a boundary condition for the integration of the flow equations. Critical points also mark the boundary between the subcritical ($F_1^2 + F_2^2 < 1$) and supercritical ($F_1^2 + F_2^2 > 1$) regimes. Only in the former can the assumption of small interfacial entrainment ($W_i \simeq 0$) be made.

Other remarkable points in the $X, h$ (phase) plane are the singular points $(X_s, h_s)$ where $P(X, h)$ and $Q(X, h)$ are simultaneously equal to zero. The configuration of the solution curves in the neighbourhood of singular points depends on the nature of the roots of the characteristic equation:

$$\lambda^2 - \lambda\left[\left(\frac{\partial P}{\partial h}\right)_s + \left(\frac{\partial Q}{\partial X}\right)_s\right] + \left(\frac{\partial P}{\partial h}\right)_s - \left(\frac{\partial P}{\partial X}\right)_s \left(\frac{\partial Q}{\partial h}\right)_s = 0. \tag{20}$$

For the simple case of equal counterflow ($\Delta q = 0$) and horizontal bottom ($\mathscr{H} = 1$), the above equation involves a single dimensionless parameter grouping: $kH/q_0 f_0$, and leads to the configuration diagram presented in figure 5. For the practical applications mentioned in § 1, the values of $kH/q_0 f_0$ are typically smaller than 0·5 so that possible singular points will be saddle or nodal points. As the solution curves of equation

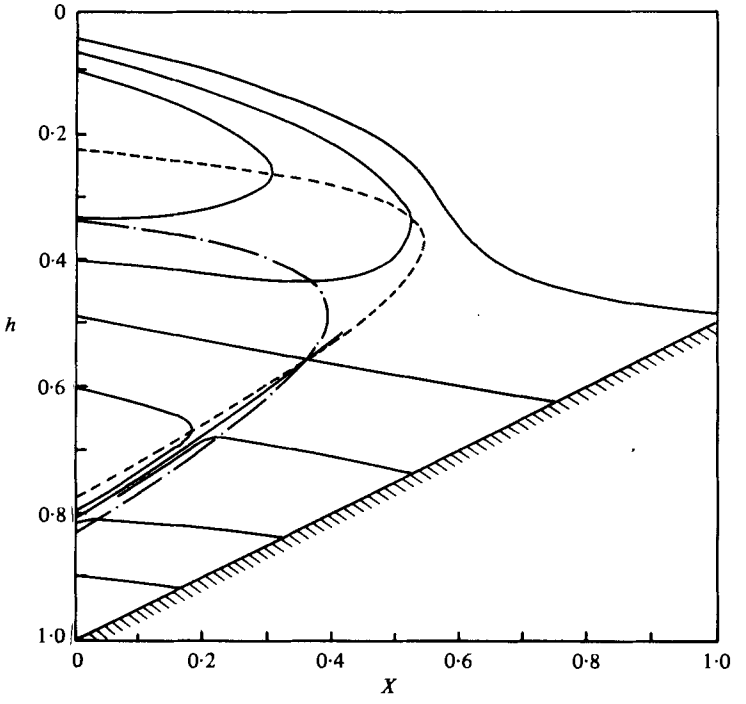


FIGURE 8. Solutions of the interface equation with a bottom slope $s = 0{\cdot}5$ and $F_E^2 = 1{\cdot}28 \times 10^{-3}$, $q_0/kL = 8, f_0 L/H = 3$. – – –, Locus of critical points; —·—, locus of points with zero interface slope.

(15) in the phase plane are shapes of layer interfaces, the foregoing conclusion is in agreement with physical requirements which preclude focuses or vortex points.

It can further be shown that, in the region of the phase plan of physical significance ($0 < h < 1$ and $r_1 > r_2$), either zero or two singular points (distinct or superposed) will exist and that, in the latter case, one will be a nodal point and the other one a saddle point. Two sets of solution curves corresponding to the above two cases are shown in figures 6 and 7. These solutions correspond to varying surface buoyancy flux as given by equation (4) and equal counterflow. The longitudinal extend, which defines $L$, is chosen so as to have $r_1 = 1$ at $X = 0$ and $r_1 = r_2$ at $X = 1$, i.e., $r_2 = \exp - kL/q_0$. With otherwise equal values of $F_E$ and of the friction parameter $f_0 L/H$, the solution without singular point presented in figure 7 corresponds to a larger value of $Q_0/kL$ and, therefore, a smaller surface buoyancy flux. For exactly zero surface buoyancy flux, the locus of points with zero interface slope completely disappears towards $X = -\infty$.

In the case of a sloping bottom, with equal counterflow, the possibility exists of zero, one, or two singular points. The locus of points with zero interface slope also has two possible shapes depending on the magnitude of the bottom slope compared to $[(1+\alpha)/\alpha_2] f_0 L/8H$. One example of each case is given in figures 8 and 9.

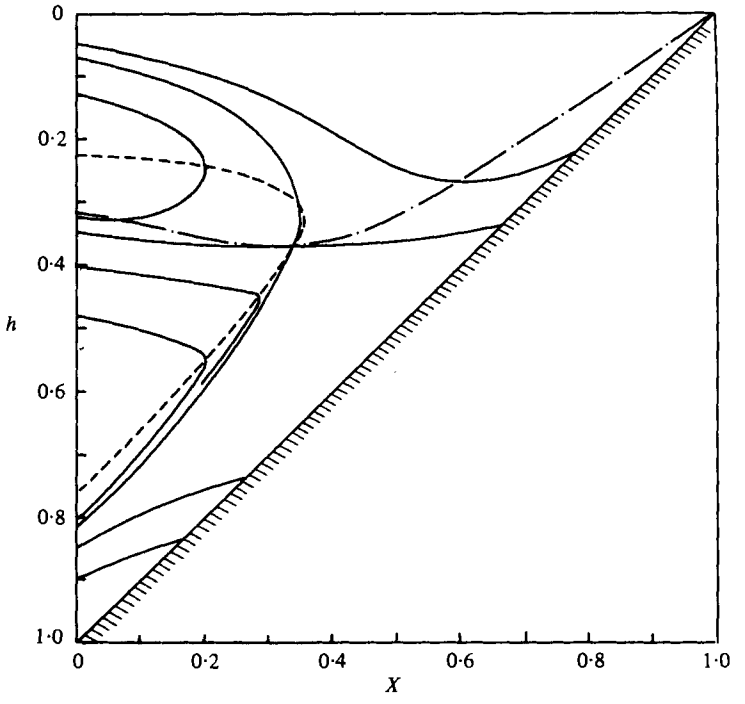


FIGURE 9. Solutions of the interface equation with a bottom slope $s = 1$ and $F_E^2 = 1{\cdot}28 \times 10^{-3}$, $q_0/kL = 8, f_0 L/H = 3$. – – –, Locus of critical points; —·—, locus of points with zero interface slope.

## 4. Two-layer convective circulation

The experimental study described in § 2 showed that for the type of shallow convective circulation under consideration, the downflow is concentrated near the closed end. A two-layer model is, therefore, applicable to the major part of the convective flow. In this region, it was shown in the previous section that the free surface elevation and the lower-layer buoyancy can be assumed constant. The latter is unknown and so is the circulation flowrate per unit width, $q_0$. In dimensionless terms, it is convenient to represent the unknown flowrate by $q_0/kL$.

The lower-layer buoyancy in the two-layer flow region depends upon the downflow distribution near the closed end. In this downflow region, the buoyancy conservation equations, (8) and (9), become:

$$q\frac{dr_1}{dX} = \frac{-BL}{q_0 b_0}, \tag{21}$$

$$-q\frac{dr_2}{dX} = \frac{dq}{dX}(r_2 - r_1), \tag{22}$$

giving

$$r_1 - r_2 = \frac{-\int_X^1 \frac{BL}{q_0 b_0}\,dX}{q}. \tag{23}$$

For the case of constant surface buoyancy flux, $B$, and for $kL/q_0(1-X) \ll 1$ if $B$ varies as given by (4), the above equation gives

$$r_1 - r_2 = -(1-X)\frac{dr_1}{dX}. \tag{24}$$

The upper-layer depth at $X = 0$ is equal to $H_u$ so that $h(X=0) = h_0 = H_u/H$. An additional condition is, however, required to allow the determination of $q_0/kL$ and of the interface shape by integration of (14).

The two-layer flow regime is expected to persist until the flow becomes unstable. The parameter governing the stability of the flow is the Richardson number (see Turner 1977); but the vertical buoyancy and velocity profiles also influence stability. Based on average layer depth and layer buoyancy difference, the Richardson number is the inverse of the square of the Froude number and the highest Froude number for stable stratified flow is of the order of unity. Therefore, in the convective circulation, the two-layer flow regime will persist until or even beyond a critical point. At such a point, the interface slope is infinite except if this critical point is also a singular point. The experimental observation pointed to an almost horizontal interface near the closed end so that it is postulated that the interface does indeed go through a singular point. This singular condition is similar to that first used by Massé (1938) for the computation of free surface flows involving the transition from subcritical to supercritical conditions resulting for instance from the steepening of the bottom slope. This application is further discussed by Chow (1959).

At the singular point, hereafter characterized by a subscript $s$, both the numerator and denominator of (14) are equal to zero. For the case of equal counterflow and introducing $K = (k^2L^2)/(b_0H^3)$, this condition gives:

$$sK\left(\frac{q_0}{kL}\right)^2 \frac{\alpha_2}{(\mathscr{H}_s - h_s)^3} - \left.\frac{dr_1}{dX}\right|_s \frac{h_s}{2} - K\left(\frac{q_0}{kL}\right)^2 \frac{f_0 L}{8H}\left[\alpha\left(\frac{1}{h_s} + \frac{1}{\mathscr{H}_s - h_s}\right)^3 + \left(\frac{1}{\mathscr{H}_s - h_s}\right)^3\right] = 0, \tag{25}$$

$$r_{1s} - r_{2s} - K\left(\frac{q_0}{kL}\right)^2 \left[\frac{\alpha_1}{h_s^3} + \frac{\alpha_2}{(\mathscr{H}_s - h_s)^3}\right] = 0. \tag{26}$$

For the case of a constant surface buoyancy flux, $dr_1/(dX)$ is a constant and if the bottom is horizontal ($s = 0$), $\mathscr{H}$ is also constant, equal to 1 if $H$ is chosen equal to the total depth. Then, if the numerator of the interface equation, (14), is equal to zero at one point, it will remain equal to zero and the solution of the problem is given by (25) with $h_s = h_0$. The interface is horizontal and the circulation flowrate is given by:

$$\frac{q_0}{kL} = \left\{K\frac{f_0 L}{H}\frac{1}{4h_0}\left[\alpha\left(\frac{1}{h_0} + \frac{1}{1-h_0}\right)^3 + \left(\frac{1}{1-h_0}\right)^3\right]\right\}^{-\frac{1}{2}}; \tag{27}$$

this can also be written

$$\frac{q_0^3}{BH^4}\frac{f_0}{4h_0}\left[\alpha\left(\frac{1}{h_0} + \frac{1}{1-h_0}\right)^3 + \left(\frac{1}{1-h_0}\right)^3\right] = 1, \tag{28}$$

according to which the circulation flowrate is independent of the length of the layer. This result is to be compared with that obtained by Phillips (1966) for the convective

circulation in the Red Sea. Using similarity arguments and a constant surface buoyancy flux, Phillips derived that the horizontal velocity is given by:

$$u = B^{\frac{1}{3}}(x-L)^{\frac{1}{3}} f(z/H) \tag{29}$$

whereby the flow continually decreases from the entrance to the closed end. This result cannot be verified directly but measured vertical buoyancy profiles closely match the expression found by Phillips:

$$b = \frac{B^{\frac{2}{3}}(L-x)^{\frac{2}{3}}}{H} g(z/H). \tag{30}$$

The horizontality of the buoyancy interface inherent in this expression derives from the assumed form of the similarity functions. The agreement with measured data, however, corroborates this point, which is one of the results of the theory proposed in this paper. The reference density used for the definition of the buoyancy, $b$, in (30) is the fluid density at the closed end of the layer. With the same definition, the expression for the surface buoyancy variation resulting from the two layer model is:

$$b_1' = \frac{B^{\frac{2}{3}}(L-x)}{H^{\frac{4}{3}} f_0^{\frac{1}{3}} \left[\frac{1}{4h_0}\left[\alpha\left(\frac{1}{h_0}+\frac{1}{1-h_0}\right)^3+\left(\frac{1}{1-h_0}\right)^3\right]\right]^{\frac{1}{3}}} \tag{31}$$

in which the buoyancy varies linearly with distance from the closed end instead of with the $\frac{2}{3}$ power of this distance as in (30). With the inevitable scatter in the measured data, either expression can be considered to agree with measurements. The present theory, however, is complete, inasmuch as it does not contain undetermined constants and comparison with the numerical values calculated by Phillips for the similarity function $g(Z/H)$ is possible. Comparing equations (30) and (31) leads to an estimate of the average of $g$ in the upper layer:

$$g_1 = \frac{(L-x)^{\frac{1}{3}}}{H^{\frac{1}{3}} f_0^{\frac{1}{3}} \left[\frac{1}{4h_0}\left[\alpha\left(\frac{1}{h_0}+\frac{1}{1-h_0}\right)^3+\left(\frac{1}{1-h_0}\right)^3\right]\right]^{\frac{1}{3}}}. \tag{32}$$

The length of the Red Sea is equal to 2400 km so that an average value of $(L-x)$ to be substituted in equation (32) is 1200 km. The depth of the entrance sill which plays a role equivalent to that of the layer depth $H$ is 120 m. A typical value of the friction factor $f_0$ is 0·02, while $h_0$ can be estimated to be approximately $\frac{1}{2}$ based on the vertical profiles presented by Phillips. These numbers lead to $g_1 = 29$ in equation (31) (with $\alpha = 0{\cdot}5$), while the function plotted by Phillips for $g(z/H)$ varies from 33 at the surface to 20 at half depth with an average of approximately 28 in the upper half. This agreement would tend to support the present theory.

For the case of varying surface buoyancy flux or for sloping bottom, a closed form solution is no longer simple. The integration of the momentum (or interface), equation (14) presents a boundary value problem with boundary conditions at $X = 0$ and at the singular point. A numerical shooting scheme was used for this integration and since the solution of the interface equation would tend to become unstable near a singular point, the adopted approach was to start integration at the singular point.

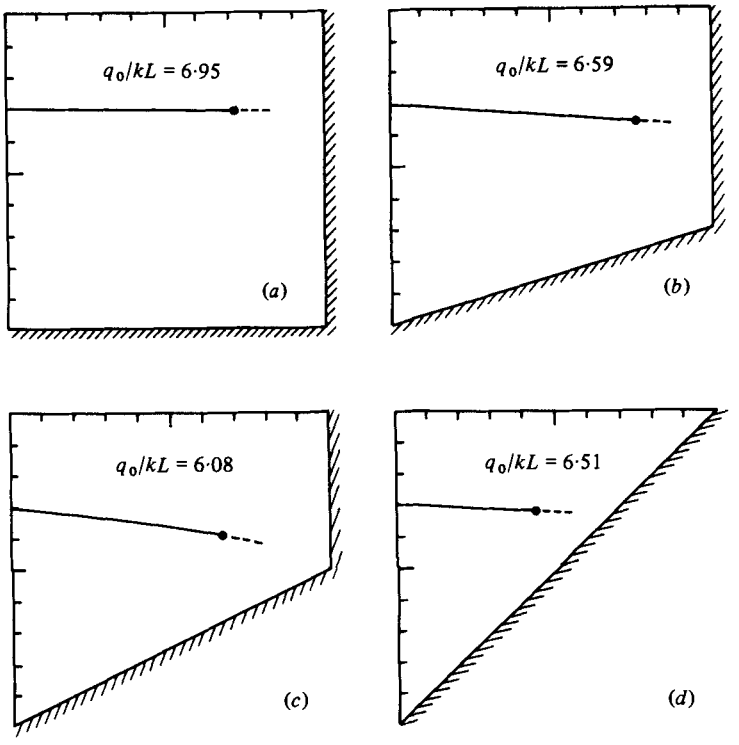


FIGURE 10. Interface profiles and circulation flowrates for increasing bottom slopes with $K = 2{\cdot}0 \times 10^{-5}$ and $f_0 L/H = 3$. (a) $s = 0$; (b) $s = 0{\cdot}3$; (c) $s = 0{\cdot}5$; (d) $s = 1{\cdot}0$.

The abscissa, $X_s$, of the singular point can be obtained from the singular condition, (25) and (26), through use of equation (24):

$$X_s = 1 + \frac{\mathscr{H}_s \dfrac{h_s^*}{2}\left[\dfrac{\alpha_1}{h_s^{*3}} + \dfrac{\alpha_2}{(1-h_s^*)^3}\right.}{s\dfrac{\alpha_2}{(1-h_s^*)^3} - \dfrac{f_0 L}{H}\left[\alpha\left(\dfrac{1}{h_s^*} + \dfrac{1}{1-h_s^*}\right)^3 + \left(\dfrac{1}{1-h_s^*}\right)^3\right]} \tag{33}$$

in which $h^* = h/\mathscr{H}$ is the relative upper layer depth and

$$\mathscr{H} = 1 - \int_0^X s\, dX.$$

If a value is assumed for $h_s^*$, $X_s$ can be calculated using the above equation and integration of the interface equation can be carried out towards $X = 0$. Startup for the numerical integration procedure requires knowledge of the limiting value of $dh/dX$ at the singular point. Using the notation of equation (20), this slope is given by the following second-degree equation.

$$\left(\frac{dh}{dx}\right)^2 \left(\frac{\partial Q}{\partial h}\right)_s + \left(\frac{dh}{dx}\right)\left[\left(\frac{\partial Q}{\partial X}\right)_s - \left(\frac{\partial P}{\partial h}\right)_s\right] - \left(\frac{\partial P}{\partial X}\right)_s = 0. \tag{34}$$

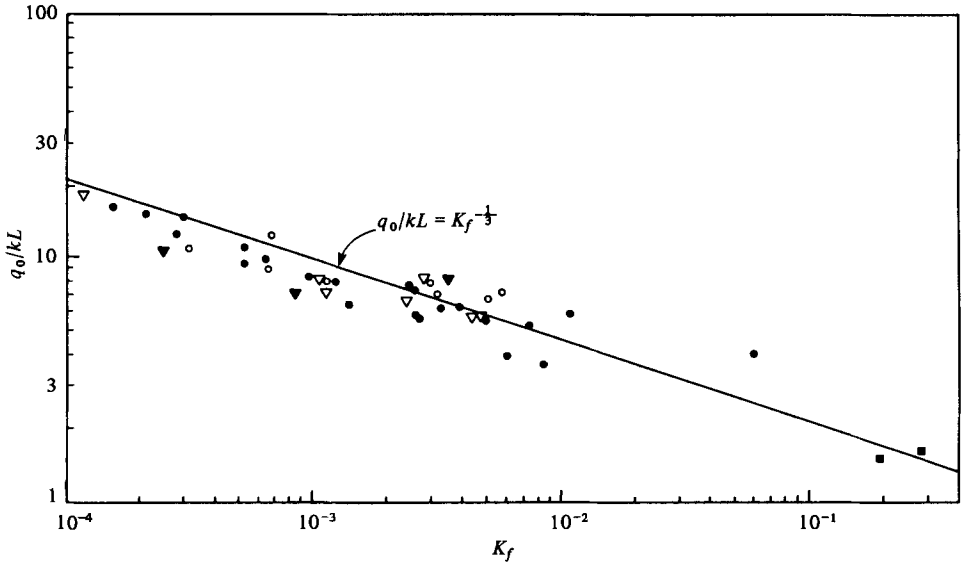


FIGURE 11. Comparison of measured convective circulation flowrates with two-layer model.

$$K_f = \frac{k^2L^2}{b_0H^3}\frac{f_0L}{H}\frac{1}{4h_0}\left[\alpha\left(\frac{1}{h_0}+\frac{1}{1-h_0}\right)^3+\left(\frac{1}{1-h_0}\right)^3\right].$$

Present study: ●, horizontal bottom, shallow upper layer; ○, horizontal bottom, deep upper layer; ▼, sloping bottom, shallow upper layer; ▽, sloping bottom, deep upper layer. Sturm (1976); ■, horizontal bottom, shallow upper layer.

This equation has the same discriminant as (20) and, therefore, has two real solutions at saddle and nodal points. Only one of these solutions points inside the subcritical region and is retained.

For varying surface buoyancy flux with horizontal bottom, the difference with the constant surface buoyancy flux solution should increase with increasing $kL/q_0$ as the longitudinal buoyancy distribution with constant surface buoyancy flux is the first term in the $kL/q_0$ equation of the varying buoyancy flux solution. For $kL/q_0$ up to 0·3, the difference between the two solutions was generally found to be less than 5 %.

For sloping bottom, the flowrate parameter, $q_0/kL$, depends independently on four parameters; $K$, $f_0L/H$, $h_0$, and $s$. It is, therefore, not possible to present general results. Interface profiles and the corresponding circulation flowrates for several uniform bottom slopes with otherwise constant values of $K, f_0L/H$, and $h_0$ are plotted in figure 10. For these values, it appears that a bottom slope results in a small reduction of the circulation flowrate. The reduction ratio does not, however, monotonously increase with increasing bottom slope. Similar qualitative results were obtained for a range of the parameters.

Another interesting feature of this model is the fact that, for $kH/q_0f_0$ less than 0·5 and for large upper-layer depths, the singular point is a nodal point through which an infinity of solution curves (interfaces) pass. The solution scheme proposed above is, therefore, indeterminate. At the same time, it was observed experimentally that for large initial upper layer depths, downflow occurred starting at $X = 0$. A solution for this case would necessarily involve the downflow distribution which cannot be predicted by the present model.

Since it was found that the circulation flowrate for varying surface buoyancy or sloping bottom varied only slightly from the constant surface buoyancy flux solution as given by equation (27), the results of the experiments described in § 2 are compared to this solution in figure 11. Also included in this comparison are data from experiments on a similar circulation performed by Sturm (1976). The agreement between measurements and the present theory is good, as much of the scatter can be explained by difficulties in the estimation of the surface buoyancy flux.

Although the present model is not applicable for large initial upper-layer depths (approximately $h_0 > 0{\cdot}5$), data points for experiments corresponding to this case have been included in figure 11. For these points, a value of $h_0 = 0{\cdot}5$ was selected for substitution in (27). Agreement with the theory remains acceptable.

## REFERENCES


Brocard, D. N., Jirka, G. H. & Harleman, D. R. F. 1977 A model for the convective circulation in side arms of cooling lakes. *Ralph M. Parsons Lab. for Water Resources & Hydrodyn., MIT, Rep.* no. 223.

Chow, V. T. 1959 *Open-Channel Hydraulics*. McGraw-Hill.

Edinger, J. R. & Geyer, J. C. 1965 Cooling water studies for Edison Electric Institute. The Johns Hopkins University, *Project* no. RP-49 – Heat Exchange in the Environment.

Hsu, S. T. & Stolzenbach, K. D. 1975 Density currents in a canal connecting stratified reservoirs. *Proc. 16th Cong. Int. Ass. for Hydraulic Res. Sao Paulo, Brasil.*

Karelse, M. 1974 Vertical exchange coefficients in stratified flows. In *Momentum and Mass Transfer in Stratified Flows* (ed. H. N. Breusens), cha. 2. (*Delft Hydraulic Lab. Rep.* R880.)

Lofquist, K. 1960 Flow and stress near an interface between stratified liquids. *Phys. Fluids* **3**, 158–175.

Long, R. R. 1975 Circulation and density distribution in a deep, strongly stratified two-layer estuary. *J. Fluid Mech.* **71**, 529–540.

Massé, P. 1938 Ressaut et ligne d'eau dans les cours d'eau a pente variable. *Rev. Gen. Hydraul. Paris* **4**, 7–11 and 61–64.

Moore, M. J. & Long, R. L. 1971 An experimental investigation of turbulent stratified shearing flow. *J. Fluid Mech.* **49**, 635–655.

Phillips, O. M. 1966 On turbulent convection currents and the circulation of the Red Sea. *Deep Sea Res.* **13**, 1149–1160.

Rigter, B. P. 1970 Density induced return current in outlet channels. *Proc. A.S.C.E., J. Hydraul. Div.* **96** (HY2), 529–546.

Ryan, P. J., Harleman, D. R. F. & Stolzenbach, K. D. 1974 Surface heat loss from cooling ponds. *Water Resources Res.* **10**, 930–938.

Schijf, J. B. & Schonfeld, J. C. 1953 Theoretical considerations on the motion of salt and fresh water. *Proc. Minnesota Int. Hydraulics Convention.*

Sturm, T. W. 1976 An analytical and experimental investigation of density currents in side arms of cooling ponds. Ph.D. thesis, Department of Mechanics and Hydraulics, University of Iowa.

Turner, J. S. 1973 *Buoyancy Effects in Fluids*. Cambridge University Press.

Welander, P. 1974 Two layer exchange in an estuary with special reference to the Baltic Sea. *J. Phys. Oceanog.* **4**, 542–556.